JCTC Journal of Chemical Theory and Computation

pubs.acs.org/JCTC Article

Impact of Diabolical Singular Points on Nonadiabatic Dynamics and a Remedy: Photodissociation of Ammonia in the First Band

Shanyu Han, Yucheng Wang, Yafu Guan, David R. Yarkony,* and Hua Guo*

Cite This: J. Chem. Theory Comput. 2020, 16, 6776−6784 Read Online

ACCESS | Metrics & More | Article Recommendations

ABSTRACT: Several recent publications have pointed out a potentially severe drawback in some widely used diabatization methods based on the electronic properties of molecules. In a diabatic representation defined by a property-based method, artificial singularities may arise due to the defining equation of the adiabatic-to-diabatic (AtD) transformation. Such diabolical singular points (DSPs) may seriously affect nuclear dynamics if they lie in the relevant configuration space. Their impact is demonstrated here using the A-band photodissociation of ammonia as an example. To this end, quantum dynamics calculations are performed based on a diabatic potential energy matrix (DPEM) constructed using the generalized Mulliken−Hush method, which is based on dipoles. These property-based results are compared with the results obtained with a DPEM determined using derivative coupling explicitly. A DSP seam is found near the Franck−Condon region, which results in a complete failure to reproduce the absorption spectrum. A modification of the generalized Mulliken−Hush method is proposed to remove the DSPs while preserving the conical intersection, which leads to an accurate reproduction of the absorption spectrum and the $NH_2(\tilde{A})/NH_2(\tilde{X})$ product branching ratio.

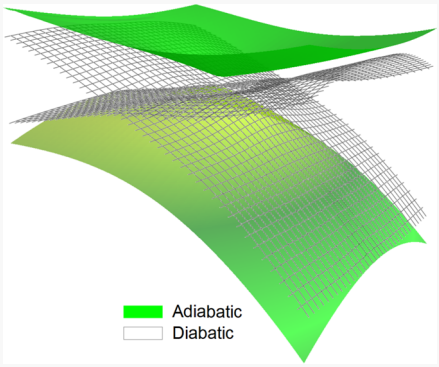

I. INTRODUCTION

The introduction of the Born−Oppenheimer (BO) adiabatic approximation[1] greatly simplified the quantum mechanical treatment of molecular systems, as it separates the electronic and nuclear motions based on their mass disparity. Indeed, modern quantum chemistry is exclusively based on the BO approximation, which allows the solution of the electronic Schrödinger equation at fixed nuclear configurations. While this approximation is often valid for dynamics on the ground electronic state, there is now increasing evidence that it breaks down due to electronic degeneracies.[2−10] A commonly encountered type of degeneracy is a conical intersection (CI),[11−13] which forms a N-2 dimensional cone-shaped crossing seam between two (sometimes more) potential energy surfaces (PESs), where N is the number of internal coordinates. Near a CI seam, the system may hop between different electronic states leading to nonadiabatic transitions. Such nonadiabatic processes are quite prevalent in photochemistry, where electronic degeneracies become rather common.[2,3,5−7,9,10] Although the adiabatic representation can in principle be used to treat nonadiabatic dynamics, it is difficult to implement in practice. This is because the derivative coupling that couples different adiabatic states is singular at the CI, and the adiabatic PESs have cusps that cannot be represented by analytical functions.[14] Furthermore, one might have to deal with the geometric phase effects if the reaction paths involve the encirclement of a CI, which could introduce interference in the adiabatic dynamics.[15−18]

A preferred alternative in dynamical calculations is the diabatic representation,[19,20] which is rigorously defined as one in which the derivative coupling is zero. In a two-state system, the two representations can be interconverted by a unitary transformation characterized by a rotational angle (Θ). In such a representation, the potential operator is represented by a matrix with diagonal and off-diagonal elements, and the diagonalization of this diabatic potential energy matrix (DPEM) gives the adiabatic PESs as its eigenvalues. In this diabatic representation, all singularities are removed and the geometric phase is implicitly included. Furthermore, all elements of a DPEM are smooth functions of the nuclear coordinates and thus amenable to analytic representation.

Unfortunately, rigorous diabatization is unattainable for molecules consisting of more than two atoms, as it would require the inclusion of all electronic states.[21,22] Consequently, a diabatic representation is often qualified by the word "quasi" because the derivative coupling is not completely removed. For this reason, the determination of the quasi-diabatic representation is not unique, and there are many different ways to make

Received: August 4, 2020
Published: September 29, 2020

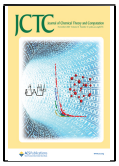

https://dx.doi.org/10.1021/acs.jctc.0c00811
J. Chem. Theory Comput. 2020, 16, 6776−6784

the adiabatic-to-diabatic (AtD) transformation.[23] These diabatizations can be crudely divided into several categories, depending on how they are constructed, including configuration uniformity,[24−26] block-diagonalization,[27,28] property-based approaches,[29−31] diabatization by ansatz,[32,33] and approaches based on an explicit calculation of derivative couplings.[20,34,35] Despite the enormity of the effort, constructing accurate DPEMs, particularly for global representations, remains a challenge in both numerical costs and operational complexity.[36]

The ab initio calculation of derivative couplings is numerically expensive, but it allows, in principle, the definition of the most accurate quasi-diabatic states, whose quality can be quantified and controlled through residual derivative couplings. In recent years, this approach has been used by several groups to construct accurate global DPEMs.[37−40] In particular, Yarkony and co-workers have proposed a simultaneous fitting and diabatization approach[41−44] and applied it to several challenging reactive systems, including NH_3,[45,46] CH_2OH,[47,48] CH_3NH_2,[49] C_6H_5OH,[50−52] and OH + H_2 systems.[53] Quantum dynamical calculations based on some of these DPEMs have successfully reproduced experimental observations and provided a more in-depth understanding of nonadiabatic dynamics.[54−64]

On the other hand, property-based diabatization methods are intuitive and provide an alternative way of diabatization at a relatively lower cost. This is because properties are much more easily calculated than derivative couplings. Taking the Boys localization (BL) diabatization described by Subotnik et al.[30] as an example, the AtD angle (Θ) is given by a tangent form: $\tan 4\Theta(\mathbf{R}) = n(\mathbf{R})/d(\mathbf{R})$, where the numerator $n(\mathbf{R})$ and denominator $d(\mathbf{R})$ are analytic functions of the molecular property operator matrix elements, which are in turn smooth functions of the nuclear coordinates $\mathbf{R}$, in the diabatic representation. In BL, the property operator is taken as the electric dipole, of which its matrix elements can be readily calculated using a quantum chemistry code. However, in a series of recent papers,[65−68] the Yarkony group has pointed out a potentially serious issue in property-based diabatization methods, namely the presence of artifactual singularities in the derivative couplings which are unrelated to true CIs. These so-called diabolical singular points (DSPs) have similar properties to a real CI and could cause a catastrophic failure of diabatization and lead to unphysical dynamics. In BL, for example, both $n(\mathbf{R})$ and $d(\mathbf{R})$ may vanish in some configurations, giving rise to such singularities.

Examples of DSPs were first shown by Zhu and Yarkony in a classic system,[65] namely the photodissociation of ammonia in its first absorption band: $NH_3(1^1\tilde{A}) + h\nu \rightarrow NH_2(\tilde{A})/NH_2(\tilde{X})$ + H. An algorithm for searching DSPs was proposed, which requires derivatives of the ab initio property used for diabatization. Using this algorithm, Wang et al. reported recently the global topography of a DSP seam in this system,[67] based on global dipole moment surfaces (DMSs) fitted with neural networks (NNs) by Guan et al.[69] Interestingly, the DSP seam was found to be located near the Franck−Condon region, and may have a severe consequence on the dissociation dynamics. However, there has so far been no investigation of the impact of DSPs on nuclear dynamics, which is the main objective of this work.

Specifically, we examine here the DSPs in the generalized Mulliken−Hush (GMH) diabatization framework,[29,70] which is similar to BL and based on electric and transition dipoles and originally designed for studying electron transfer. Taking advantage of the NN DMSs of Guan et al.,[69] we construct the GMH DPEM and show that a DSP seam exists near the Franck−Condon region of the $NH_3(1^1\tilde{A}) + h\nu \rightarrow NH_2(\tilde{A})/NH_2(\tilde{X})$ + H system. Full-dimensional quantum dynamics based on the GHM DPEM reveals a complete failure of this DPEM in reproducing the absorption spectrum, due to the DSPs. This issue is expected to be present in other property-based diabatization scheme such as BL, so quite general. To mitigate the problem, a modified GMH scheme is proposed, which eliminates the DSP, but preserves the CI crossing. This new diabatization scheme is shown to correctly reproduce the absorption spectrum as well as the branching ratio between the $NH_2(\tilde{X})$ + H and $NH_2(\tilde{A})$ + H channels caused by nonadiabatic dynamics via a planar CI. This work is organized as follows. Section II briefly reviews the original GMH method and the associated DSPs, introduces the modified GMH method, and outlines the quantum dynamical method. The results and discussions are given in Section III. The conclusion is given in Section IV.

II. THEORY

II.I. Transformation between Adiabatic and Diabatic States. In a common two-state model, the transformation between the adiabatic states $\Psi_\alpha^{(a)}(\mathbf{R};\mathbf{q})$ (α = 1,2) and diabatic states $\Psi_I^{(d)}(\mathbf{R};\mathbf{q})$ (I = 1,2) is given by a unitary transformation, namely a rotation in the Hilbert space

$$\begin{pmatrix}\Psi_1^{(d)}(\mathbf{r};\mathbf{R})\\ \Psi_2^{(d)}(\mathbf{r};\mathbf{R})\end{pmatrix} = \begin{pmatrix}\cos\Theta(\mathbf{R}) & \sin\Theta(\mathbf{R})\\ -\sin\Theta(\mathbf{R}) & \cos\Theta(\mathbf{R})\end{pmatrix}\begin{pmatrix}\Psi_1^{(a)}(\mathbf{r};\mathbf{R})\\ \Psi_2^{(a)}(\mathbf{r};\mathbf{R})\end{pmatrix} \quad (1)$$

where $\mathbf{r}$ and $\mathbf{R}$ are electronic and nuclear coordinates, respectively, and $\Theta(\mathbf{R})$ is the adiabatic-to-diabatic (AtD) rotational angle, which itself is a function of the nuclear coordinates. Note that the superscript $(a)/(d)$ denotes the adiabatic/diabatic representation (the same goes for other definitions below). The adiabatic derivative coupling, $\mathbf{f}_{12}^{(a)}(\mathbf{R}) \equiv \langle\Psi_1^{(a)}(\mathbf{r};\mathbf{R})|\nabla_R\Psi_2^{(a)}(\mathbf{r};\mathbf{R})\rangle_{\mathbf{r}}$, can be evaluated by the derivative of the AtD angle $\Theta(\mathbf{R})$ and the diabatic derivative coupling $\mathbf{f}_{12}^{(d)}(\mathbf{R})$

$$\mathbf{f}_{12}^{(a)}(\mathbf{R}) = \nabla_R\Theta(\mathbf{R}) + \mathbf{f}_{12}^{(d)}(\mathbf{R}) \quad (2)$$

In a rigorous diabatic representation, $\mathbf{f}_{12}^{(d)}(\mathbf{R})$ is zero, but in a quasi-diabatic representation, it cannot be completely eliminated. In such a case, we have

$$\mathbf{f}_{12}^{(a)}(\mathbf{R}) = \nabla_R\Theta(\mathbf{R}) \quad (3)$$

In the diabatic representation, the potential operator is expressed as DPEM, which is related to the adiabatic energies via the same unitary transformation

$$\begin{aligned}&\begin{pmatrix}V_{11}^{(d)}(\mathbf{R}) & V_{12}^{(d)}(\mathbf{R})\\ V_{12}^{(d)}(\mathbf{R}) & V_{22}^{(d)}(\mathbf{R})\end{pmatrix}\\ &= \begin{pmatrix}\cos\Theta(\mathbf{R}) & \sin\Theta(\mathbf{R})\\ -\sin\Theta(\mathbf{R}) & \cos\Theta(\mathbf{R})\end{pmatrix}\begin{pmatrix}E_1^{(a)}(\mathbf{R}) & 0\\ 0 & E_2^{(a)}(\mathbf{R})\end{pmatrix}\\ &\quad\times\begin{pmatrix}\cos\Theta(\mathbf{R}) & -\sin\Theta(\mathbf{R})\\ \sin\Theta(\mathbf{R}) & \cos\Theta(\mathbf{R})\end{pmatrix}\end{aligned} \quad (4)$$

https://dx.doi.org/10.1021/acs.jctc.0c00811
J. Chem. Theory Comput. 2020, 16, 6776−6784

Below, the superscripts in the potentials will be dropped as they are self-evident.

II.II. Generalized Mulliken−Hush Diabatization. In the generalized Mulliken−Hush (GMH) theory of Cave and Newton,[29,70] the diabatization is based on the dipole operator $\hat{\boldsymbol{\mu}} = (\hat{\mu}^x, \hat{\mu}^y, \hat{\mu}^z)$. The diabatic elements of the dipole matrix are defined as

$$\mu_{IJ}^{(d)}(\mathbf{R}) = \langle \Psi_I^{(d)}(\mathbf{R}) | (\hat{\mu}^x, \hat{\mu}^y, \hat{\mu}^z) | \Psi_J^{(d)}(\mathbf{R}) \rangle_r \tag{5}$$

Their relationship with the adiabatic matrix elements, $\vec{\mu}_{\alpha\beta}^{(a)}(\mathbf{R})$, which can be defined analogously, is given as follows in a two-state model[29]

$$\vec{\mu}_{11}^{(d)} = \sin 2\Theta \vec{\mu}_{12}^{(a)} + (\cos^2\Theta \vec{\mu}_{11}^{(a)} + \sin^2\Theta \vec{\mu}_{22}^{(a)}) \tag{6a}$$

$$\vec{\mu}_{22}^{(d)} = -\sin 2\Theta \vec{\mu}_{12}^{(a)} + (\sin^2\Theta \vec{\mu}_{11}^{(a)} + \cos^2\Theta \vec{\mu}_{22}^{(a)}) \tag{6b}$$

$$\vec{\mu}_{12}^{(d)} = \cos 2\Theta \vec{\mu}_{12}^{(a)} - 1/2 \sin 2\Theta (\vec{\mu}_{11}^{(a)} - \vec{\mu}_{22}^{(a)}) \tag{6c}$$

The GMH diabatization was originally designed for electron transfer, which involves the migration of a charge from a donor to an acceptor.[29,70] This charge transfer is directional and can be conveniently defined in such a system by the unit vector $\vec{\nu} = (\vec{\mu}_{11}^{(a)} - \vec{\mu}_{22}^{(a)})/|\vec{\mu}_{11}^{(a)} - \vec{\mu}_{22}^{(a)}|$. The diabatization is thus based on the projection of the dipoles along this direction. In the two-state GMH theory, the projection is given as $\mu_{12}^{(p),\nu} = \vec{\mu}_{12}^{(p)} \cdot \vec{\nu}$ (p = a, d, and the superscript ν denotes the direction $\vec{\nu}$), and eq 6c becomes

$$\mu_{12}^{(d),\nu} = \cos 2\Theta \mu_{12}^{(a),\nu} - \frac{1}{2} \sin 2\Theta |\vec{\mu}_{11}^{(a)} - \vec{\mu}_{22}^{(a)}| \tag{7}$$

As $\mu_{12}^{(d),\nu} = 0$ defines the diabatic representation in GMH theory,[29,70] the rotation angle can be obtained from eq 7

$$\tan 2\Theta(\mathbf{R}) = n(\mathbf{R})/d(\mathbf{R}) \tag{8a}$$

with the numerator and denominator given as

$$n(\mathbf{R}) = 2\mu_{12}^{(a),\nu} \tag{8b}$$

$$d(\mathbf{R}) = |\vec{\mu}_{11}^{(a)} - \vec{\mu}_{22}^{(a)}| \tag{8c}$$

We can rewrite the derivative coupling in eq 3 in terms of $n(\mathbf{R})$ and $d(\mathbf{R})$ as

$$\nabla_R \Theta(\mathbf{R}) = -\frac{d(\mathbf{R})\nabla_R n(\mathbf{R}) - n(\mathbf{R})\nabla_R d(\mathbf{R})}{4n(\mathbf{R})^2 + d(\mathbf{R})^2} \tag{9}$$

Equations 8a and 9 are singular when $n(\mathbf{R}) = d(\mathbf{R}) = 0$. Such singular points are referred as diabolical singular points (DSPs).[65] As shown by Subotnik et al., GMH is a special case of BL.[30] Hence, the discussion here also applies to BL diabatization. As discussed below, the existence of these DSPs can have a dramatic impact on diabatization and nonadiabatic dynamics.

II.III. Modified Generalized Mulliken−Hush (mGMH) Diabatization. As has been suggested in ref 66 and implemented successfully in ref 71, these DSPs can be removed by introducing a simple energy-dependent factor $(E_1 - E_2)^2\omega^2$ in the denominator $d(\mathbf{R})$, which can prevent $n(\mathbf{R})$ and $d(\mathbf{R})$ from simultaneously vanishing when $E_1 \neq E_2$. Addition of this term is equivalent to adding a fourth component $\omega\hat{H}_{el}$ to the dipole operator. Here, ω is an adjustable parameter and $\hat{H}_{el}$ is the electronic Hamiltonian. A similar parameter has recently been introduced to optimize diabatic states.[72] At the real CI seam where $E_1 = E_2$, this term vanishes and has thus no effect. Based on this idea, we present below a modified GMH (mGMH) method for diabatization.

As suggested earlier,[66] a new four-component vector operator in mGMH can be defined as $\hat{\boldsymbol{\Omega}} = (\hat{\Omega}^{(1)}, \hat{\Omega}^{(2)}, \hat{\Omega}^{(3)}, \text{and } \hat{\Omega}^{(4)})$, with its elements in the diabatic representation as

$$\Omega_{IJ}^{(d),i} = \langle \Psi_I^{(d)}(\mathbf{R}) | \hat{\Omega}^{(i)} | \Psi_J^{(d)}(\mathbf{R}) \rangle_r \tag{10}$$

Following the GMH diabatization, $\hat{\Omega}^{(i\,=\,1,2,3)} = \hat{\mu}^{(x,y,z)}$ are the three components of dipole, but the fourth component here is defined as

$$\hat{\Omega}^{(4)} = \omega\hat{H}_{el} \tag{11}$$

Its adiabatic matrix elements are given as

$$\Omega_{11}^{(a),(4)} = \omega E_1, \quad \Omega_{22}^{(a),(4)} = \omega E_2, \quad \Omega_{12}^{(a),(4)} = 0 \tag{12}$$

In this current mGMH method, the new direction for projection can be defined as

$$\nu' = \nu_0/|\nu_0| \text{ with } \nu_0 = (\nu_0^{(1)}, \nu_0^{(2)}, \nu_0^{(3)}, \nu_0^{(4)}), \text{ and } \nu_0^{(i)} = C_0^{(i)}(\Omega_{11}^{(a),i} - \Omega_{22}^{(a),i}) \tag{13}$$

where $C_0^{(1-3)}$ are prefactors chosen to make the diabatization go smoothly and $C_0^{(4)} = 1$. Projecting the dipoles eq 6a−6c into the new direction $\vec{\nu}'$, we can arrive at an expression for the AtD angle analogous to that defined in the original GMH method

$$\tan 2\Theta = n(\mathbf{R})/d(\mathbf{R}) = \frac{2\nu' \cdot \Omega_{12}^{(a)}}{\nu' \cdot (\Omega_{11}^{(a)} - \Omega_{22}^{(a)})} \tag{14}$$

Here, the dot product involves all four components. Making full use of eq 12 and defining the normalization factor $1/|\vec{\nu}_0|$ as γ, we can express eq 14 explicitly in terms of dipole components and energies

$$\tan 2\Theta = \frac{2\sum_{i=1}^{4} \gamma C_{12}^{(i)} (\Omega_{11}^{(a),i} - \Omega_{22}^{(a),i}) \Omega_{12}^{(a),i}}{\sum_{i=1}^{4} \gamma C_{12}^{(i)} (\Omega_{11}^{(a),i} - \Omega_{22}^{(a),i})^2} = \frac{2\sum_{i=1}^{3} \gamma C_{12}^{(i)} (\mu_{11}^{(a),i} - \mu_{22}^{(a),i}) \mu_{12}^{(a),i}}{\sum_{i=1}^{3} \gamma C_{12}^{(i)} (\mu_{11}^{(a),i} - \mu_{22}^{(a),i})^2 + (E_1 - E_2)^2 \omega^2 \gamma} \tag{15}$$

which can be given in a more compact way

$$\tan 2\Theta = \frac{2\vec{\nu} \cdot \vec{\mu}_{12}^{(a)}}{\vec{\nu} \cdot (\vec{\mu}_{11}^{(a)} - \vec{\mu}_{22}^{(a)}) + (E_1 - E_2)^2 \omega^2 \gamma} \tag{16}$$

where the dot product runs only over the three components of dipoles. Importantly, the inclusion of the $(E_1 - E_2)^2\omega^2\gamma$ term in the denominator removes the DSP. Note that this term has no impact on the CI, where it vanishes because of $E_1 = E_2$. When $C_{12}^{(i)\,=\,1,2,3} = 1$ and $\omega = 0$, eq 16 recovers eq 8a−8c, namely the original GMH.

In practice, to obtain the correct AtD angle Θ from eq 16, one has to deal with the geometric phase produced by the CI.[15−18] When moving along a closed path encircling the CI, the AtD angle Θ will change by π, resulting in a significant change in the electronic wave function ($e^{i\pi} = -1$).[20] Consequently, the most general solution to eq 8a is required, which is[71]

https://dx.doi.org/10.1021/acs.jctc.0c00811
J. Chem. Theory Comput. 2020, 16, 6776−6784

$$\Theta = \frac{a\tan 2[n(\mathbf{R}),\, d(\mathbf{R})] + k\pi}{2} \quad (17)$$

where $a\tan2[n(\mathbf{R}),d(\mathbf{R})]$ is the two-argument inverse tangent function and k is a manually adjustable integer being 0 or ±1 to account for all possible values of Θ. Its treatment in practice is discussed in more detail below.

It should be mentioned that in this work the parameters chosen for the mGMH DPEM are $\omega = 8$, $C_0^{(i)=1,2,3} = 10$, 1, and 1. Other choices may also work, but this set of parameters is sufficient for our purpose. We used a neural network (NN) with two hidden layers and 20 neurons in each hidden layer to fit the global AtD angle, more importantly, to determine the value of k based on continuity (vide infra). For a discussion of NN fitting of ab initio data, the reader is referred to the recent review.[36]

II.IV. Quantum Dynamics. The photodissociation dynamics of ammonia (NH_3) in its first absorption band is characterized in this work by a wave packet method[10] with a diabatic nuclear Hamiltonian ($J = 0$) defined in the Jacobi–Radau coordinates (r_1,r_2,R,θ_1,θ_2,ϕ), as shown in Figure 1. The initial wave packet in the excited $\tilde{A}$ state is defined by the wave function of the lowest vibrational states in the $\tilde{X}$ state with even parity, and odd parity the tunneling doublet is not included as it behaves similarly. The six-dimensional excited-state wave packet was propagated using the Chebyshev propagator[73] on the specified DPEM. The absorption spectrum was obtained by Fourier transfer of the Chebyshev autocorrelation function, and the branching ratio was determined by a flux method. For details of the discretization, propagation, and calculations of the observables, the reader is referred to our previous publications.[54,55]

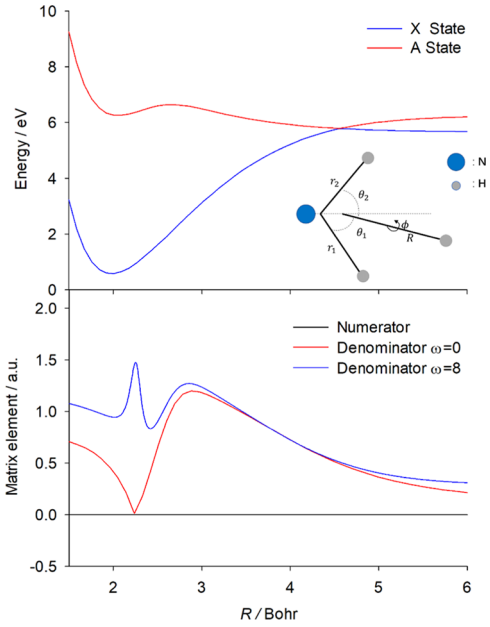

Figure 1. Upper panel: Cuts of the adiabatic PESs (E_1 and E_2) as a function of R within the planar geometry with the rest of the coordinates fixed at the ground-state geometry. Lower panel: The numerator and denominator of the tangent function of the AtD angle as the function of R for $\omega = 0$ and $\omega = 8$, where the other coordinates are fixed as $r_1 = 1.94$ Bohr, $r_2 = 2.09$ Bohr, $\theta_1 = 129.06°$, $\theta_2 = 109.15°$, and $\phi = 180°$. Note that the numerator in both cases is equal to zero by symmetric requirement.

III. RESULTS AND DISCUSSION

III.I. Effects of DSPs on Potential Energy Surfaces and Couplings. The construction of the GMH and mGMH DPEMs requires the adiabatic energies of the two states, as well as the AtD transformation matrix. The former was taken from Zhu–Yarkony (ZY) 2 × 2 DPEM for ammonia,[45,46] with the eigenvalues yielding the two adiabatic energies. The latter is determined by the AtD mixing angle, which is, in turn, obtained from dipole functions in GMH, augmented with adiabatic energies in mGMH, as shown in eqs 8a–8c and 17, respectively. The dipoles as a function of the nuclear coordinates are obtained from the recent work of Guan et al.,[69] in which the components of both the permanent and transition dipoles were fit in a diabatic representation. This way, we avoid explicit quantum chemical calculations of both energies and dipoles.

DSPs in the GMH DPEM are found in the regions of nuclear coordinate space distinct from those found in the BL diabatization, as they are determined by distinct defining equations. However, prominent DSPs in the GMH DPEM are located at planar geometries, similar to the well-established DSPs found in the BL diabatization as reported in a recent work.[67] Importantly, these DSPs are due to the symmetry of the system, which provides one of the two constraints that define the N-2 dimensional seam of DSPs. Specifically, the numerator $n(\mathbf{R}) = 2\mu_{12}^{(a),v} = \vec{\mu}_{12}^{(a)}\cdot(\vec{\mu}_{11}^{(a)} - \vec{\mu}_{22}^{(a)})/|\vec{\mu}_{11}^{(a)} - \vec{\mu}_{22}^{(a)}|$ vanishes at planar geometries, where $\mu_{11}^{(a),z} = \mu_{22}^{(a),z} = 0$ and $\mu_{12}^{(a),y} = \mu_{12}^{(a),x} = 0$. Here, the planar molecule is placed in $x - y$ plane. Within planarity, the denominator $d(\mathbf{R}) = |\vec{\mu}_{11}^{(a)} - \vec{\mu}_{22}^{(a)}|$ may accidentally equal to zero. Indeed, such a DSP has been found near the Franck–Condon region. This is shown in Figure 1, in which both the numerator and denominator are plotted as a function of H–NH_2 distance R as the molecule is constrained within the planar geometry ($\phi = 180°$) and the remaining coordinates are $r_1 = 1.94$ Bohr, $r_2 = 2.09$ Bohr, $\theta_1 = 129.06°$, and $\theta_2 = 109.15°$. In the same figure, cuts of the adiabatic PES are also shown, and it is clear that the DSP is near the Franck–Condon region.

Figure 2 displays the diagonal (V_{11} and V_{22}) and off-diagonal (V_{12}) elements of the GMH ($\omega = 0$) DPEM and mGMH ($\omega = 8$) DPEMs. These figures are plotted in the R and ϕ (out-of-plane angle). The discontinuities can be clearly seen at $R = 2.2$ Bohr, $\phi = 180°$, which corresponds to the DSP mentioned above. It is also clear that the elements of the DPEM are all strongly affected by this DSP in its vicinity.

In the mGMH DPEM with $\omega = 8$, this DSP is removed, yielding a smooth DPEM without singularities, as shown by the corresponding DPEM elements in Figure 2. The comparison between $\omega = 0$ and 8 can be more clearly seen from the AtD angle in Figure 3. The AtD angle in the GMH ($\omega = 0$) diabatization exhibits two peaks pointing to opposite directions near the DSP, which gives rise to a sudden change in the AtD angle. However, the angle is smooth for the mGMH ($\omega = 8$) diabatization in the same region, although there are still some fluctuations in the AtD angle, but no singularity. It should be noted that the $(E_1 - E_2)^2\omega^2\gamma$ factor not only precludes a zero denominator at $R = 2.2$ Bohr, but also makes it much larger than the numerator in regions where the energy difference $(E_2 - E_1)$ is large. As a result, $a\tan2[n(\mathbf{R}),d(\mathbf{R})]$ is very small, and the AtD angle varies near $\Theta = 0, \pm90°$, which makes the diabatic states coincide with the adiabatic states when the adiabatic states are well separated. However, the

https://dx.doi.org/10.1021/acs.jctc.0c00811
J. Chem. Theory Comput. 2020, 16, 6776–6784

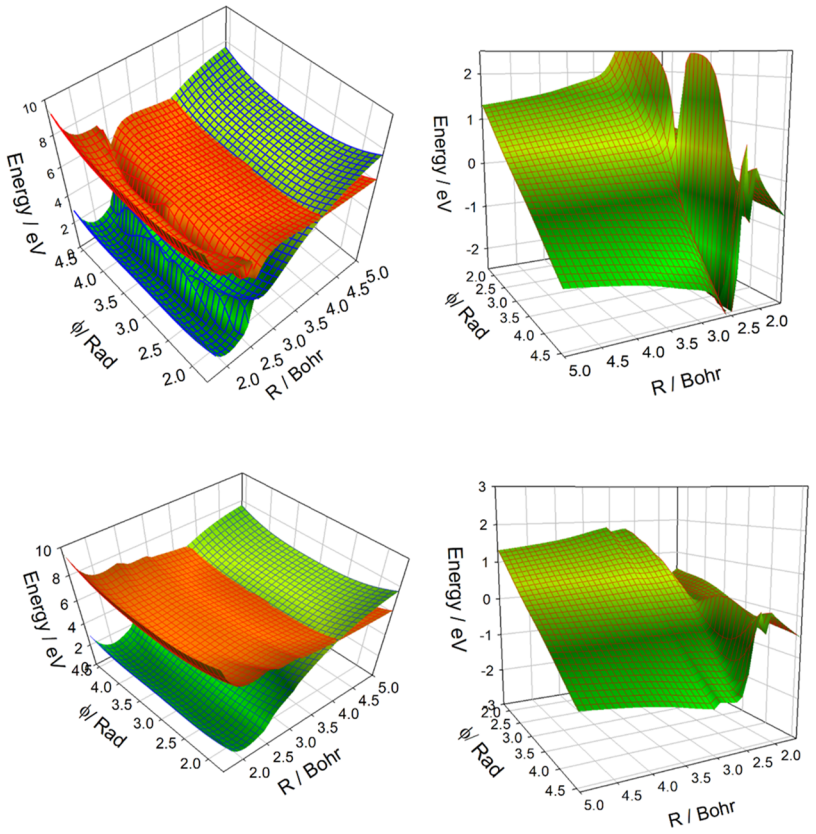

Figure 2. Comparison of the diagonal terms V_{11}, V_{22} (left), and off-diagonal term V_{12} (right) of the $\omega = 0$ (upper panel, GMH) and $\omega = 8$ (lower panel, mGMH) DPEMs.

DPEM elements in mGMH might differ significantly from that of a DPEM determined by explicit minimizing the derivative coupling, but they all give the same adiabatic PESs. This underscores the nonuniqueness of diabatization.

III.II. Determination of Θ: Continuity and the Geometric Phase. As discussed above, the determination of the AtD angle Θ near the CI seam requires some special treatment. Figure 4 illustrates how the parameter k should be chosen. First, the AtD angle Θ needs to be continuous. In Figure 4a,b, ϕ = 174°, and 186°, respectively, while the rest of the coordinates are fixed at r_1 = 1.87 Bohr, r_2 = 1.87 Bohr, θ_1 = 107°, and θ_2 = 107°. It is clear that the angle computed directly from the inverse tangent function $a\tan2[n(\mathbf{R}),d(\mathbf{R})]$ (dashed blue line) is discontinuous near R = 4.5 Bohr. To maintain continuity, according to eq 17, $k\pi/2$ should be added. Adding $-\pi/2$ after R = 4.5 Bohr in Figure 4a and $\pi/2$ in Figure 4b leads to a smooth and continuous curve for Θ. Second, the AtD angle Θ must satisfy a constraint imposed by the geometry phase that encirclement of the CI results in a change by π. As there is a portion of CI seam located at planar geometries, corresponding to $\phi = \pi$ in this defined coordinate system, Θ has to be antisymmetric with respect to $\phi = \pi$. This is illustrated in Figure 4c, where the dependence of Θ on R and ϕ near the CI is shown. The curves in Figure 4a,b are highlighted by the red lines. For $\phi < \pi$, Θ varies from 0 to $-\pi/2$ as R increases, while for $\phi > \pi$, it changes from 0 to $\pi/2$. Importantly, the fitting only covers the half region for $\phi < \pi$ to avoid the double valued Θ at $\phi = \pi$ outside the CI, and its values in the other half of the angular range are obtained by antisymmetrization.

It is also acceptable for Θ to vary from $\pi/2$ $(-\pi/2)$ to 0 for $\phi < \pi$ $(\phi > \pi)$ as R passing through the CI, which means adding $\pi/2$ $(-\pi/2)$ before R = 4.5 Bohr in Figure 4a (Figure 4b). The resultant diagonal terms of DPEM V_{11} and V_{22} would in this case resemble the adiabatic excited-state E_2 and ground-state E_1, respectively, the small R region, and switch to E_1 and E_2 in the large R region. However, this option was not chosen as V_{11} and V_{22} are conventionally referred to as the ground and excited states in the Franck−Condon region.

We note here in passing that the current approach guarantees the exact reproduction of the adiabatic energies. An alternative approach is to fit directly the elements of the DPEM, as done recently by many investigators,[74−76] which will not give the exact adiabatic energies due to fitting errors, but it avoids the double-valuedness of the AtD angle.

III.III. Effects of DSPs on the Absorption Spectrum. Figure 5 displays the absorption spectrum calculated using the GMH ($\omega = 0$) DPEM, which is compared with the result from the ZY DPEM. The peaks on the GMH DPEM are broad and shifted, with no resemblance to the narrow and regularly spaced peaks obtained from the ZY DPEM, which are known to agree with the experiment quite well.[45] It is well established that the sharp peaks stem from the pyramidal-to-planar excitation, which places the wave packet in a pyramidal geometry on the excited-state PES, which has a planar equilibrium geometry. The subsequent dynamics is thus dominated by oscillation along the umbrella (ν_2) coordinate. However, as shown in Figure 2, the excited-state PES in the GMH DPEM is strongly affected by the DSP, leading to completely wrong dynamics. This example highlights the detrimental impact of DSPs on excited-state dynamics.

https://dx.doi.org/10.1021/acs.jctc.0c00811
J. Chem. Theory Comput. 2020, 16, 6776−6784

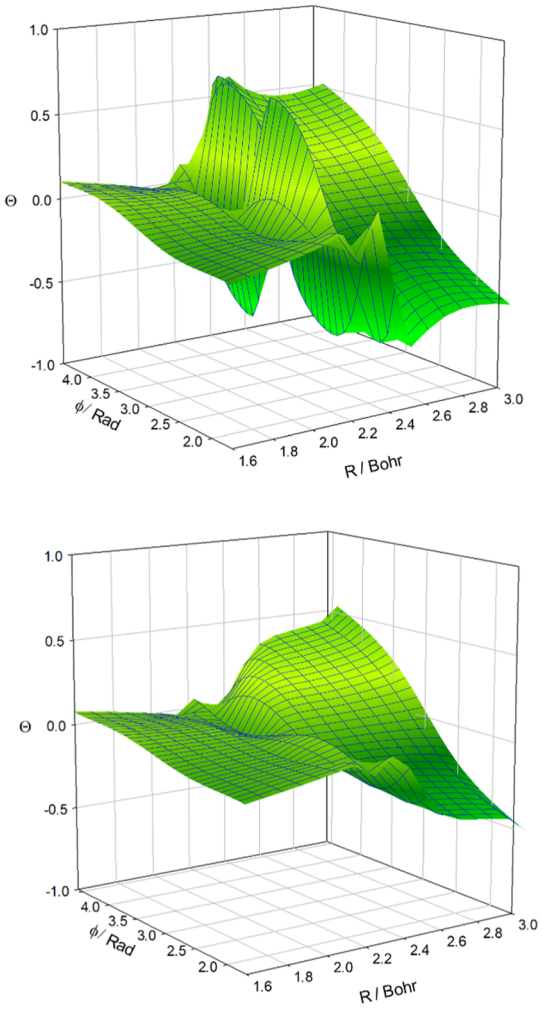

Figure 3. Comparison of the AtD angle for the $\omega = 0$ (upper panel, GMH) and $\omega = 8$ (lower panel, mGMH) DPEMs near the DSP.

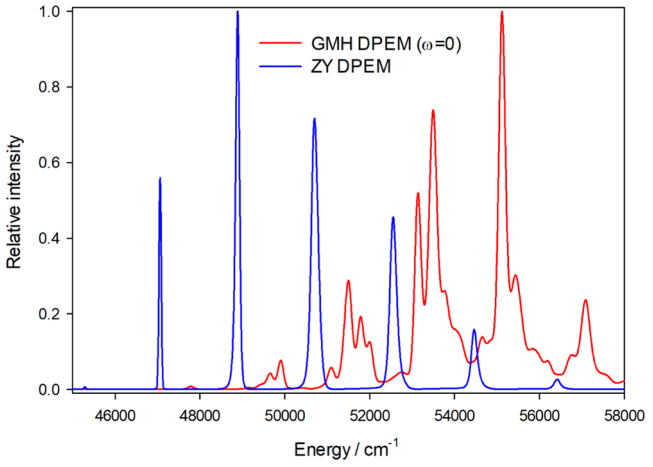

Figure 5. Comparison of the absorption spectrum calculated with the GMH ($\omega = 0$) and ZY DPEMs. Note that only the energy peaks of even parity peaks are shown here.

III.IV. Absorption Spectrum and Branching Ratio from mGMH DPEM. The removal of the DSP by the mGMH diabatization demonstrated in Figure 5 is expected to remedy the problem discussed in the above section. Indeed, it can be seen from Figure 6 that the calculated absorption spectrum using the mGMH ($\omega = 8$) DPEM yields an excellent agreement with that calculated using the ZY DPEM. This indicates that the dynamics in the Franck−Condon region is correctly described by the mGMH DPEM. As discussed above, however, the excited-state PES in this region is sufficiently separated from the ground-state PES, far away from the CI seam where nonadiabatic transitions take place.

In the photodissociation of ammonia, the wave packet exiting the Franck−Condon region will encounter a CI, as shown in Figure 1. Nonadiabatic transitions near the CI lead to the production of both the $NH_2(\tilde{A})$ + H and $NH_2(\tilde{X})$ + H products. To further examine the accuracy of the mGMH DPEM in describing the nonadiabatic dynamics near the CI seam, the $NH_2(\tilde{A})/NH_2(\tilde{X})$ product branching ratio was calculated and is compared with that calculated from the ZY DPEM in Figure 6. The overall agreement between the two is excellent, although there are still some quantitative differences. This general agreement underscores the correct description of the nonadiabatic coupling of the mGMH DPEM near the CI seam, where nonadiabatic transitions take place. The small differences are most likely due to the fitting errors in both the dipole and the mixing angle. Given the fact that the branching ratio is very sensitive to the DPEM, this level of agreement demonstrates the reliability of the proposed mGMH method in diabatization and in the construction of the DPEM.

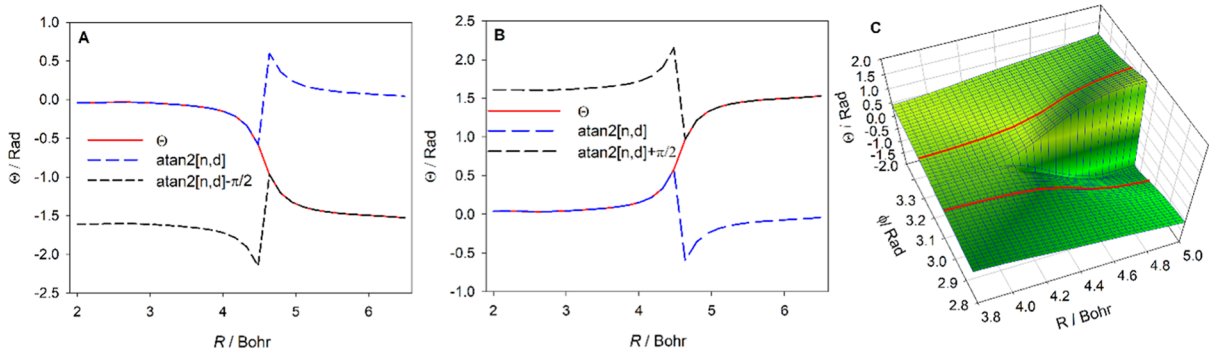

Figure 4. (A) Comparison of the mGMH ($\omega = 8$) AtD angle Θ (red line) obtained from inversed tangent function $a\tan2[n, d]$ (blue dashed line) and $a\tan2[n, d] - \pi/2$ (black dashed line) as functions of R with the rest of the coordinates fixed at $r_1 = 1.87$ Bohr, $r_2 = 1.87$ Bohr, $\theta_1 = 107°$, $\theta_2 = 107°$, and $\phi = 174°$. (B) The same as A but $\phi = 186°$ and $a\tan2[n, d] + \pi/2$ (black dashed line). (C) the mGMH ($\omega = 8$) AtD angle Θ in the two-dimensional space of R and ϕ. The red lines highlight the Θ shown in the left and middle panels.

https://dx.doi.org/10.1021/acs.jctc.0c00811
J. Chem. Theory Comput. 2020, 16, 6776−6784

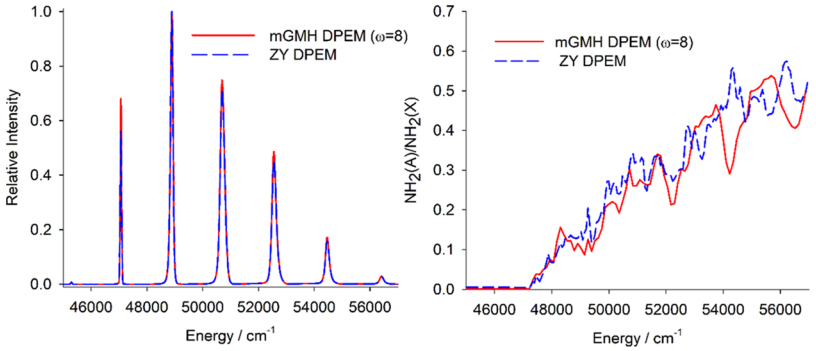

Figure 6. Comparison of the absorption spectrum (the left panel) and product branching ratio (the right panel) calculated with the mGMH (ω = 8) DPEM and ZY DPEM. Note that only even parity peaks are shown here.

IV. CONCLUSIONS

In this work, we have demonstrated the deleterious dynamical consequences that emerge when DSPs go undetected in a property-based diabatization, including BL or GMH approaches. In the case of ammonia, such singular points form a *N*-2 dimensional seam lying in the Franck−Condon region due to symmetry reasons. The detrimental effects on the dynamics are striking. A simple remedy is proposed to remove this singularity, and at the same time, preserve the CI seam and its geometric phase effect. The mGMH diabatization is shown to reproduce both the absorption spectrum, which is dominated by the excited-state dynamics in the Franck−Condon region, and the product branching ratio, which is controlled by nonadiabatic dynamics near the CI seam. This strategy can be applied to other property-based diabatization schemes affected by DSPs. As a result, this less expensive diabatization can be used to diabatize and to construct DPEMs for nonadiabatic dynamics.

AUTHOR INFORMATION

Corresponding Authors

David R. Yarkony − *Department of Chemistry, Johns Hopkins University, Baltimore, Maryland 21218, United States;* orcid.org/0000-0002-5446-1350; Email: yarkony@jhu.edu

Hua Guo − *Department of Chemistry and Chemical Biology, University of New Mexico, Albuquerque, New Mexico 87131, United States;* orcid.org/0000-0001-9901-053X; Email: hguo@unm.edu

Authors

Shanyu Han − *Department of Chemistry and Chemical Biology, University of New Mexico, Albuquerque, New Mexico 87131, United States*

Yucheng Wang − *Department of Chemistry, Johns Hopkins University, Baltimore, Maryland 21218, United States*

Yafu Guan − *Department of Chemistry, Johns Hopkins University, Baltimore, Maryland 21218, United States*

Complete contact information is available at: https://pubs.acs.org/10.1021/acs.jctc.0c00811

Notes

The authors declare no competing financial interest.

ACKNOWLEDGMENTS

This work was supported by the Department of Energy (DE-SC0015997 to H.G. and National Science Foundation grant CHE 1954723 to D.R.Y.). The main calculations were performed at the Center for Advanced Research Computing (CARC) at UNM and at the National Energy Research Scientific Computing (NERSC) Center.

REFERENCES

(1) Born, M.; Huang, K. *Dynamical Theory of Crystal Lattices*; Clarendon: Oxford, 1954.

(2) Bernardi, F.; Olivucci, M.; Robb, M. A. Potential energy surface crossings in organic photochemistry. *Chem. Soc. Rev.* **1996**, *25*, 321−328.

(3) Worth, G. A.; Cederbaum, L. S. Beyond Born-Oppenheimer: Molecular dynamics through a conical intersection. *Annu. Rev. Phys. Chem.* **2004**, *55*, 127−158.

(4) Jasper, A. W.; Nangia, S.; Zhu, C.; Truhlar, D. G. Non-Born−Oppenheimer molecular dynamics. *Acc. Chem. Res.* **2006**, *39*, 101−108.

(5) Levine, B. G.; Martínez, T. J. Isomerization through conical intersections. *Annu. Rev. Phys. Chem.* **2007**, *58*, 613−634.

(6) Matsika, S.; Krause, P. Nonadiabatic events and conical intersections. *Annu. Rev. Phys. Chem.* **2011**, *62*, 621−643.

(7) Yarkony, D. R. Nonadiabatic quantum chemistry—past, present and future. *Chem. Rev.* **2011**, *112*, 481−498.

(8) Tully, J. C. Perspective: Nonadiabatic dynamics theory. *J. Chem. Phys.* **2012**, *137*, No. 22A301.

(9) Domcke, W.; Yarkony, D. R. Role of conical intersections in molecular spectroscopy and photoinduced chemical dynamics. *Annu. Rev. Phys. Chem.* **2012**, *63*, 325−352.

(10) Guo, H.; Yarkony, D. R. Accurate nonadiabatic dynamics. *Phys. Chem. Chem. Phys.* **2016**, *18*, 26335−26352.

(11) Köuppel, H.; Domcke, W.; Cederbaum, L. S. Multimode molecular dynamics beyond the Born-Oppenheimer approximation. *Adv. Chem. Phys.* **1984**, *57*, 59−246.

(12) Yarkony, D. R. Diabolical conical intersections. *Rev. Mod. Phys.* **1996**, *68*, 985−1013.

(13) Domcke, W.; Yarkony, D. R.; Köppel, H. *Conical Intersections: Electronic Structure, Dynamics and Spectroscopy*; World Scientific: Singapore, 2004.

(14) Yarkony, D. R.; Xie, C.; Zhu, X.; Wang, Y.; Malbon, C. L.; Guo, H. Diabatic and adiabatic representations: Electronic structure caveats. *Comput. Theor. Chem.* **2019**, *1152*, 41−52.

(15) Mead, C. A. The geometric phase in molecular systems. *Rev. Mod. Phys.* **1992**, *64*, 51−85.

(16) Kendrick, B. K. Geometric phase effects in chemical reaction dynamics and molecular spectra. *J. Phys. Chem. A* **2003**, *107*, 6739−6756.

(17) Ryabinkin, I. G.; Joubert-Doriol, L.; Izmaylov, A. F. Geometric phase effects in nonadiabatic dynamics near conical intersections. *Acc. Chem. Res.* **2017**, *50*, 1785−1793.

(18) Xie, C.; Malbon, C. L.; Guo, H.; Yarkony, D. R. Up to a sign. The insidious effects of energetically inaccessible conical intersections on unimolecular reactions. *Acc. Chem. Res.* **2019**, *52*, 501−509.
(19) Smith, F. T. Diabatic and adiabatic representations for atomic collision problems. *Phys. Rev.* **1969**, *179*, 111−123.
(20) Baer, M. *Beyond Born-Oppenheimer: Electronic Nonadiabatic Coupling Terms and Conical Intersections*; Wiley: New Jersey, 2006.
(21) Mead, C. A.; Truhlar, D. G. Conditions for the definition of a strictly diabatic electronic basis for molecular systems. *J. Chem. Phys.* **1982**, *77*, 6090−6098.
(22) Baer, M. Adiabatic and diabatic representations for atom-diatom collisions: Treatment of the three-dimensional case. *Chem. Phys.* **1976**, *15*, 49−57.
(23) Köppel, H. Diabatic Representation Methods for the Construction of Diabatic Electronic States. In *Conical Intersections: Electronic Structure, Dynamics and Spectroscopy*; Domcke, W.; Yarkony, D. R.; Köppel, H., Eds.; World Scientific: Singapore, 2004.
(24) Atchity, G. J.; Ruedenberg, K. Determination of diabatic states through enforcement of configurational uniformity. *Theor. Chem. Acc.* **1997**, *97*, 47−58.
(25) Nakamura, H.; Truhlar, D. G. Direct diabatization of electronic states by the fourfold way. II. Dynamical correlation and rearrangement processes. *J. Chem. Phys.* **2002**, *117*, 5576−5593.
(26) Nakamura, H.; Truhlar, D. G. Extension of the fourfold way for calculation of global diabatic potential energy surfaces of complex, multiarrangement, non-Born−Oppenheimer systems:Application to HNCO(S_0,S_1). *J. Chem. Phys.* **2003**, *118*, 6816−6829.
(27) Pacher, T.; Cederbaum, L. S.; Köppel, H. Approximately diabatic states from block diagonalization of the electronic Hamiltonian. *J. Chem. Phys.* **1988**, *89*, 7367−7381.
(28) Pacher, T.; Cederbaum, L. S.; Köppel, H. Adiabatic and quasidiabatic states in a gauge theoretical framework. *Adv. Chem. Phys.* **1993**, *84*, 293−391.
(29) Cave, R. J.; Newton, M. D. Calculation of electronic coupling matrix elements for ground and excited state electron transfer reactions: Comparison of the generalized Mulliken−Hush and block diagonalization methods. *J. Chem. Phys.* **1997**, *106*, 9213−9226.
(30) Subotnik, J. E.; Yeganeh, S.; Cave, R. J.; Ratner, M. A. Constructing diabatic states from adiabatic states: Extending generalized Mulliken−Hush to multiple charge centers with Boys localization. *J. Chem. Phys.* **2008**, *129*, No. 244101.
(31) Hoyer, C. E.; Parker, K.; Gagliardi, L.; Truhlar, D. G. The DQ and DQΦ electronic structure diabatization methods: Validation for general applications. *J. Chem. Phys.* **2016**, *144*, No. 194101.
(32) Lenzen, T.; Manthe, U. Neural network based coupled diabatic potential energy surfaces for reactive scattering. *J. Chem. Phys.* **2017**, *147*, No. 084105.
(33) Williams, D. M. G.; Eisfeld, W. Neural network diabatization: A new ansatz for accurate high-dimensional coupled potential energy surfaces. *J. Chem. Phys.* **2018**, *149*, No. 204106.
(34) Baer, M. Adiabatic and diabatic representations for atom-molecule collisions: Treatment of the collinear arrangement. *Chem. Phys. Lett.* **1975**, *35*, 112−118.
(35) Top, Z. H.; Baer, M. Incorporation of electronically nonadiabatic effects into bimolecular reactive systems. I. Theory. *J. Chem. Phys.* **1977**, *66*, 1363−1371.
(36) Jiang, B.; Li, J.; Guo, H. High-fidelity potential energy surfaces for gas phase and gas-surface scattering processes from machine learning. *J. Phys. Chem. Lett.* **2020**, *11*, 5120−5131.
(37) Evenhuis, C. R.; Collins, M. A. Interpolation of diabatic potential energy surfaces. *J. Chem. Phys.* **2004**, *121*, 2515−2527.
(38) Godsi, O.; Evenhuis, C. R.; Collins, M. A. Interpolation of multidimensional diabatic potential energy matrices. *J. Chem. Phys.* **2006**, *125*, No. 104105.
(39) Ghosh, S.; Mukherjee, S.; Mukherjee, B.; Mandal, S.; Sharma, R.; Chaudhury, P.; Adhikari, S. Beyond Born-Oppenheimer theory for ab initio constructed diabatic potential energy surfaces of singlet H_3^+ to study reaction dynamics using coupled 3D time-dependent wave-packet approach. *J. Chem. Phys.* **2017**, *147*, No. 074105.
(40) Yuan, D.; Guan, Y.; Chen, W.; Zhao, H.; Yu, S.; Luo, C.; Tan, Y.; Xie, T.; Wang, X.; Sun, Z.; et al. Observation of the geometric phase effect in the H + HD → H_2 + D reaction. *Science* **2018**, *362*, 1289−1293.
(41) Zhu, X.; Yarkony, D. R. Toward eliminating the electronic structure bottleneck in nonadiabatic dynamics on the fly: An algorithm to fit nonlocal, quasidiabatic, coupled electronic state Hamiltonians based on ab initio electronic structure data. *J. Chem. Phys.* **2010**, *132*, No. 104101.
(42) Zhu, X.; Yarkony, D. R. On the representation of coupled adiabatic potential energy surfaces using quasi-diabatic Hamiltonians: A distributed origins expansion approach. *J. Chem. Phys.* **2012**, *136*, No. 174110.
(43) Guan, Y.; Guo, H.; Yarkony, D. R. Neural network based quasi-diabatic Hamiltonians with symmetry adaptation and a correct description of conical intersections. *J. Chem. Phys.* **2019**, *150*, No. 214101.
(44) Guan, Y.; Zhang, D. H.; Guo, H.; Yarkony, D. R. Representation of coupled adiabatic potential energy surfaces using neural network based quasi-diabatic Hamiltonians: 1,2 $^2A'$ states of LiFH. *Phys. Chem. Chem. Phys.* **2019**, *21*, 14205−14213.
(45) Zhu, X.; Ma, J.; Yarkony, D. R.; Guo, H. Computational determination of the $\tilde{A}$ state absorption spectrum of NH_3 and of ND_3 using a new quasi-diabatic representation of the $\tilde{X}$ and $\tilde{A}$ states and full six-dimensional quantum dynamics. *J. Chem. Phys.* **2012**, *136*, No. 234301.
(46) Zhu, X.; Yarkony, D. R. Quasi-diabatic representations of adiabatic potential energy surfaces coupled by conical intersections including bond breaking: A more general construction procedure and an analysis of the diabatic representation. *J. Chem. Phys.* **2012**, *137*, No. 22A511.
(47) Malbon, C. L.; Yarkony, D. R. On the nonadiabatic photodissociation of the hydroxymethyl radical from the 2^2A State. Surface hopping simulations based on a full nine dimensional representation of the 1,2,3^2A potential energy surfaces coupled by conical intersections. *J. Phys. Chem. A* **2015**, *119*, 7498−7509.
(48) Malbon, C. L.; Yarkony, D. R. Multistate, multichannel coupled diabatic state representations of adiabatic states coupled by conical intersections. CH_2OH photodissociation. *J. Chem. Phys.* **2017**, *146*, No. 134302.
(49) Wang, Y.; Xie, C.; Guo, H.; Yarkony, D. R. A quasi-diabatic representation of the 1,2^1A states of methylamine. *J. Phys. Chem. A* **2019**, *123*, 5231−5241.
(50) Zhu, X.; Yarkony, D. R. Fitting coupled potential energy surfaces for large systems: Method and construction of a 3-state representation for phenol photodissociation in the full 33 internal degrees of freedom using multireference configuration interaction determined data. *J. Chem. Phys.* **2014**, *140*, No. 024112.
(51) Zhu, X.; Malbon, C. L.; Yarkony, D. R. An improved quasi-diabatic representation of the 1, 2, 3^1A coupled adiabatic potential energy surfaces of phenol in the full 33 internal coordinates. *J. Chem. Phys.* **2016**, *144*, No. 124312.
(52) Zhu, X.; Yarkony, D. R. On the elimination of the electronic structure bottleneck in on the fly nonadiabatic dynamics for small to moderate sized (10-15 atom) molecules using fit diabatic representations based solely on ab initio electronic structure data: The photodissociation of phenol. *J. Chem. Phys.* **2016**, *144*, No. 024105.
(53) Malbon, C. L.; Zhao, B.; Guo, H.; Yarkony, D. R. On the nonadiabatic collisional quenching of OH(A) by H_2: a four coupled quasi-diabatic state description. *Phys. Chem. Chem. Phys.* **2020**, *22*, 13516−13527.
(54) Ma, J.; Zhu, X.; Guo, H.; Yarkony, D. R. First principles determination of the NH_2/ND_2(A/X) branching ratios for photodissociation of NH_3/ND_3 via full-dimensional quantum dynamics based on a new quasi-diabatic representation of coupled ab initio potential energy surface. *J. Chem. Phys.* **2012**, *137*, No. 22A541.
(55) Ma, J.; Xie, C.; Zhu, X.; Yarkony, D. R.; Xie, D.; Guo, H. Full-dimensional quantum dynamics of vibrationally mediated photo-

https://dx.doi.org/10.1021/acs.jctc.0c00811
J. Chem. Theory Comput. 2020, 16, 6776−6784

dissociation of NH_3 and ND_3 on coupled ab initio potential energy surfaces: Absorption spectra and $NH_2(\tilde{A}^2A_1)/NH_2(\tilde{X}^2B_1)$ branching ratios. *J. Phys. Chem. A* **2014**, *118*, 11926−11934.
(56) Xie, C.; Ma, J.; Zhu, X.; Zhang, D. H.; Yarkony, D. R.; Xie, D.; Guo, H. Full-dimensional quantum state-to-state non-adiabatic dynamics for photodissociation of ammonia in its A-band. *J. Phys. Chem. Lett.* **2014**, *5*, 1055−1060.
(57) Xie, C.; Zhu, X.; Ma, J.; Yarkony, D. R.; Xie, D.; Guo, H. Communication: On the competition between adiabatic and nonadiabatic dynamics in vibrationally mediated ammonia photodissociation in its A band. *J. Chem. Phys.* **2015**, *142*, No. 091101.
(58) Xie, C.; Ma, J.; Zhu, X.; Yarkony, D. R.; Xie, D.; Guo, H. Nonadiabatic tunneling in photodissociation of phenol. *J. Am. Chem. Soc.* **2016**, *138*, 7828−7831.
(59) Xie, C.; Kendrick, B. K.; Yarkony, D. R.; Guo, H. Constructive and destructive Interference in nonadiabatic tunneling via conical intersections. *J. Chem. Theory Comput.* **2017**, *13*, 1902−1910.
(60) Xie, C.; Malbon, C.; Yarkony, D. R.; Guo, H. Nonadiabatic photodissociation dynamics of the hydroxymethyl radical via the $2^2A(3s)$ Rydberg state: A four-dimensional quantum study. *J. Chem. Phys.* **2017**, *146*, No. 224306.
(61) Xie, C.; Malbon, C. L.; Yarkony, D. R.; Guo, H. Dynamic mapping of conical intersection seams: A general method for incorporating the geometric phase in adiabatic dynamics in polyatomic systems. *J. Chem. Phys.* **2017**, *147*, No. 044109.
(62) Xie, C.; Malbon, C. L.; Yarkony, D. R.; Xie, D.; Guo, H. Signatures of a conical intersection in adiabatic dissociation on the ground electronic state. *J. Am. Chem. Soc.* **2018**, *140*, 1986−1989.
(63) Xie, C.; Malbon, C. L.; Xie, D.; Yarkony, D. R.; Guo, H. Nonadiabatic dynamics in photodissociation of hydroxymethyl in the $3^2A(3p_x)$ Rydberg state: A nine-dimensional quantum study. *J. Phys. Chem. A* **2019**, *123*, 1937−1944.
(64) Xie, C.; Zhao, B.; Malbon, C. L.; Yarkony, D. R.; Xie, D.; Guo, H. Insights into the mechanism of nonadiabatic photodissociation from product vibrational distributions. The remarkable case of phenol. *J. Phys. Chem. Lett.* **2020**, *11*, 191−198.
(65) Zhu, X.; Yarkony, D. R. On the construction of property based diabatizations: Diabolical singular points. *J. Phys. Chem. A* **2015**, *119*, 12383−12391.
(66) Zhu, X.; Yarkony, D. R. Constructing diabatic representations using adiabatic and approximate diabatic data—Coping with diabolical singularities. *J. Chem. Phys.* **2016**, *144*, No. 044104.
(67) Wang, Y.; Guan, Y.; Yarkony, D. R. On the impact of singularities in the two-state adiabatic to diabatic state transformation: A global treatment. *J. Phys. Chem. A* **2019**, *123*, 9874−9880.
(68) Wang, Y.; Yarkony, D. R. Determining whether diabolical singularities limit the accuracy of molecular property based diabatic representations: The 1,21A states of methylamine. *J. Chem. Phys.* **2018**, *149*, No. 154108.
(69) Guan, Y.; Guo, H.; Yarkony, D. R. Extending the representation of multistate coupled potential energy surfaces to include properties operators using neural networks: Application to the $1,2^1A$ states of ammonia. *J. Chem. Theory Comput.* **2020**, *16*, 302−313.
(70) Cave, R. J.; Newton, M. D. Generalization of the Mulliken-Hush treatment for the calculation of electron transfer matrix elements. *Chem. Phys. Lett.* **1996**, *249*, 15−19.
(71) Guan, Y.; Yarkony, D. R. Accurate neural network representation of the ab initio determined spin−orbit Interaction in the diabatic representation including the effects of conical intersections. *J. Phys. Chem. Lett.* **2020**, *11*, 1848−1858.
(72) Alguire, E.; Subotnik, J. E. Optimal diabatic states based on solvation parameters. *J. Chem. Phys.* **2012**, *137*, No. 194108.
(73) Guo, H. A time-independent theory of photodissociation based on polynomial propagation. *J. Chem. Phys.* **1998**, *108*, 2466−2472.
(74) Yang, K. R.; Xu, X.; Zheng, J. J.; Truhlar, D. G. Full-dimensional potentials and state couplings and multidimensional tunneling calculations for the photodissociation of phenol. *Chem. Sci.* **2014**, *5*, 4661−4580.
(75) Guan, Y.; Fu, B.; Zhang, D. H. Construction of diabatic energy surfaces for LiFH with artificial neural networks. *J. Chem. Phys.* **2017**, *147*, No. 224307.
(76) Xie, C.; Zhu, X.; Yarkony, D. R.; Guo, H. Permutation invariant polynomial neural network approach to fitting potential energy surfaces. IV. Coupled diabatic potential energy matrices. *J. Chem. Phys.* **2018**, *149*, No. 144107.

https://dx.doi.org/10.1021/acs.jctc.0c00811
J. Chem. Theory Comput. 2020, 16, 6776−6784